Clinical applications of perfluorocarbon nanoparticles for molecular imaging and targeted therapeutics

Trung D Tran[1]
Shelton D Caruthers[1,2]
Michael Hughes[1]
John N Marsh[1]
Tillmann Cyrus[1]
Patrick M Winter[1]
Anne M Neubauer[1]
Samuel A Wickline[1]
Gregory M Lanza[1]

[1]Division of Cardiology, Washington University Medical School, 660 South Euclid Blvd, St Louis, Missouri, USA; [2]Philips Medical Systems, Cleveland, Ohio, USA

Abstract: Molecular imaging is a novel tool that has allowed non-invasive diagnostic imaging to transition from gross anatomical description to identification of specific tissue epitopes and observation of biological processes at the cellular level. This technique has been confined to the field of nuclear imaging; however, recent advances in nanotechnology have extended this research to include ultrasound (US) and magnetic resonance (MR) imaging. The exploitation of nanotechnology for MR and US molecular imaging has generated several candidate contrast agents. One multimodality platform, targeted perfluorocarbon (PFC) nanoparticles, is useful for noninvasive detection with US and MR, targeted drug delivery, and quantification.

Keywords: nanoparticles, perfluorocarbon, molecular imaging, ultrasound, magnetic resonance imaging

Introduction

Recent advances in genomics, proteomics and molecular biology have created an unprecedented opportunity to identify clinical pathology in their "pre-disease" states. Unfortunately, detection of small aggregates of dysplastic cells and their biochemical signatures are beyond the resolution and sensitivity of conventional acoustic and magnetic resonance imaging techniques. Recognition of these molecular epitopes requires target-specific probes, a robust signal amplification strategy and a sensitive high-resolution imaging modality.

Numerous nano- or micro-particle systems are in development for targeted diagnostic imaging and drug delivery, which have been recently reviewed (Cyrus et al in press). The perfluorocarbon (PFC) nanoparticle is a unique platform technology, which may be applied to clinically relevant modalities and illustrates many of the key principles found in other agents. Ligand-directed, lipid-encapsulated, liquid PFC nanoparticles (250 nm nominal diameter) have inherent physicochemical properties, which provide acoustic contrast when the agent is bound in aggregate to a surface. High surface area of the nanoparticle accommodates 50 to 500 homing ligands, which imparts high avidity and gives the agent a robust "stick and stay" quality (see Figure 1). Surface incorporation of large payloads of lipid-gadolinium chelate conjugates further extends the utility of the agent to detect sparse concentrations of cell surface biochemical markers with MRI (Lanza, Lorenz et al 1998). Moreover, the high fluorine signal from the nanoparticle core allows noninvasive quantification of ligand-bound particles, which will permit clinicians to confirm tissue concentrations of drugs when functionality of the nanoparticles is extended to include targeted therapy (see Figure 2).

The definition of nanoparticle is varied based on the perspective and historical timeframe. In the materials section of the NIH and NSF, the size of nanoparticles defined by a change in the properties of structures, particularly with respect to their quantum features for optical imaging. The NCI and NHLBI typically refer to nanoparticles in their RFAs for biomedical applications at 300 nm and the Europeans use a 500 nm

Correspondence: Gregory M Lanza
Associate Professor of Medicine and Bioengineering, Division of Cardiology, Washington University Medical School, 660 S. Euclid Ave, Campus Box 8086, Saint Louis, MO 63110, USA
Tel +1 314 454 8813
Fax +1 314 454 5265
Email greg@cvu.wustl.edu

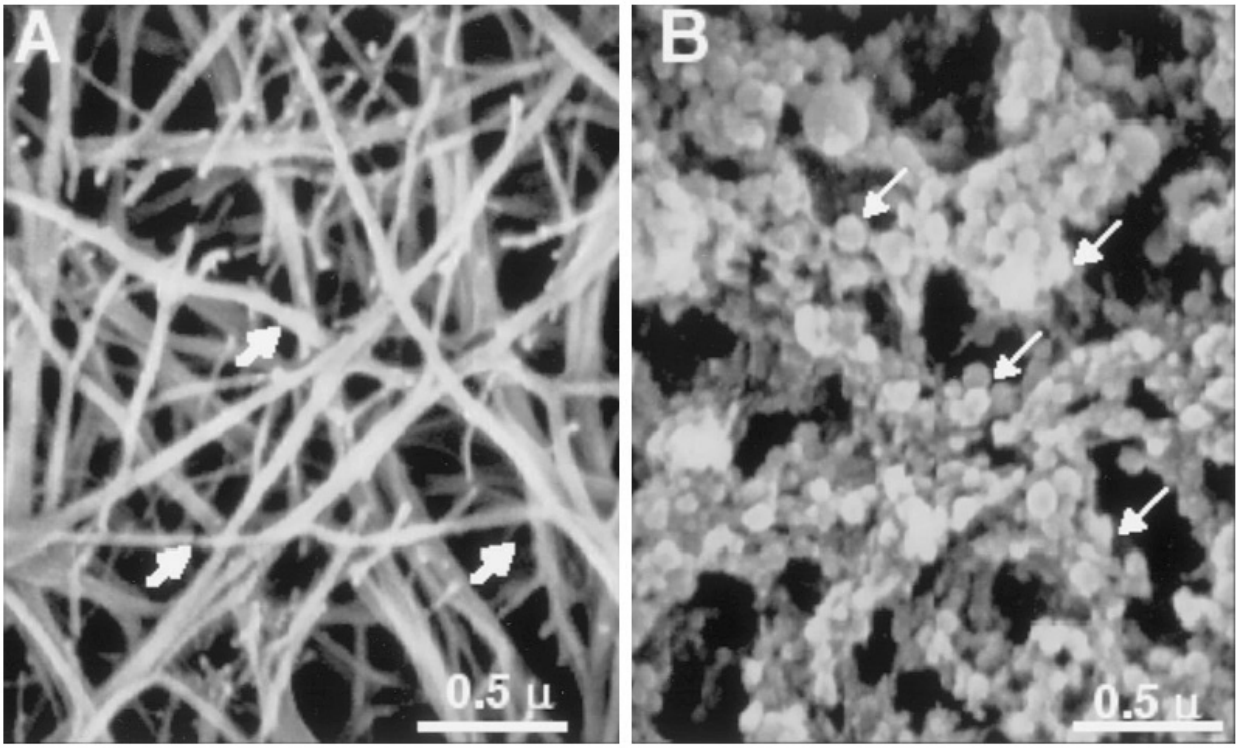

Figure 1 Scanning electron micrographs (x30 000) of control fibrin clot (**A**) and fibrin-targeted paramagnetic nanoparticles bound to the clot surface (**B**). Arrows indicate (**A**) fibrin fibril; (**B**) fibrin-specific nanoparticles-bound to fibrin epitopes. Copyright © 2001. Reprinted with permission from Flacke S, Fischer S, et al. 2001. Novel MRIM contrast agent for molecular imaging of fibrin: implications for detecting vulnerable plaques. *Circulation*, 104:1280–5.

cut-off. In biomedical applications, the surface to volume ratio and the pharmacokinetics and biodistribution features of nanoparticles are the important qualities. Although the majority of nanoparticles are synthetic using natural products or polymers, there are contingents of scientists that encouraging the NIH to include engineered viruses as nanoparticles! Thus in reality, the definition of nanoparticle in the biological sciences is dynamic, referring to particles generally less than 500 nm and typically, though not exclusively, chemically synthesized or fabricated.

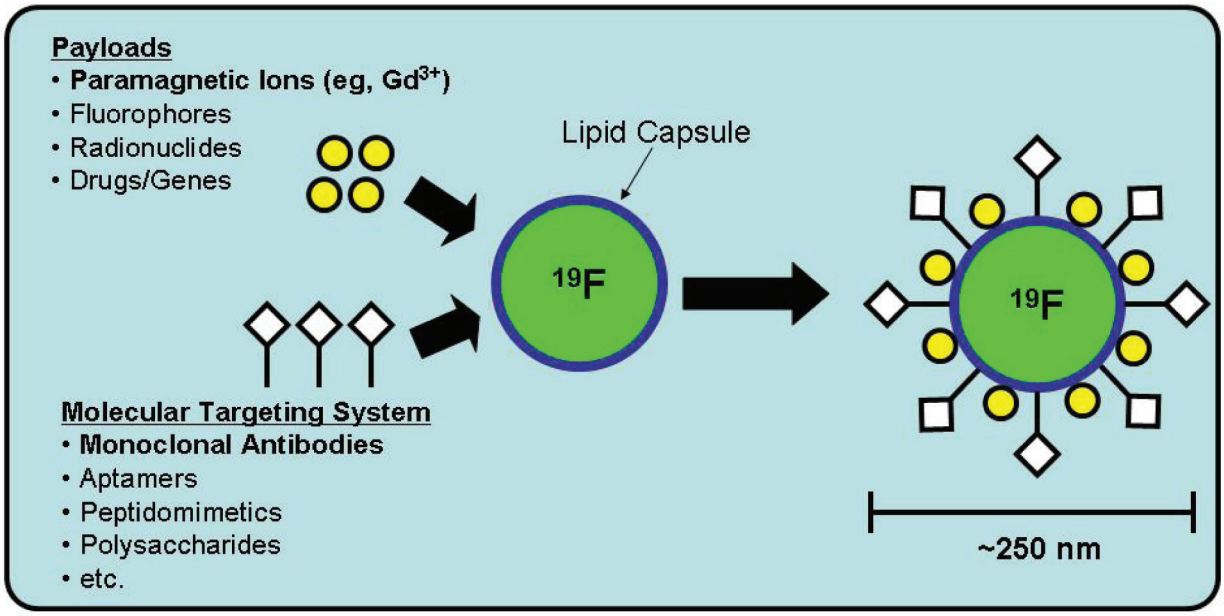

Figure 2 Paradigm for targeted liquid perfluorocarbon-based nanoparticle contrast agents. This example has a payload of Gd^{3+} chelates and monoclonal antibodies. This platform is extremely versatile and applicable to almost any imaging modalities and capable of carrying other payloads such as drugs or genes.

Targeted versus non-targeted contrast agents

Localization of non-targeted contrast agents depends greatly upon the body's innate system for clearance of foreign particles, ie, the reticuloendothelial system (RES). Macrophages of the RES are responsible for the removal of these contrast agents from the circulation, which occurs in a size-dependent fashion from the lung, spleen, liver and bone marrow. Furthermore, phagocytosis and accumulation within specific sites can be enhanced by opsonization (ie, biologic tagging) with blood proteins such as immunoglobins, complement proteins or nonimmune serum factors. In general, liver sequestration appears to be complement mediated, while the spleen removes foreign particulate matter via antibody Fc receptors (Moghimi and Patel 1989). This process of nonspecific and nondirected uptake of particles is generally referred to as "passive targeting".

Ligand-directed ("targeted") contrast agents are designed to identify specific pathological tissue that otherwise might be difficult to distinguish from surrounding normal tissue. A wide variety of ligands can be utilized including monoclonal antibodies and fragments, peptides, polysaccharides, aptamers and drugs. These ligands may be attached covalently (ie, direct conjugation) or non-convalently (ie, indirect conjugation) to the contrast agent. Further surface modification, such as the incorporation of polyethylene glycol, are used to delay or avoid rapid systemic removal of the agents and allow ligand-to-target binding to occur. To demonstrate the effectiveness of this concept of targeting contrast agents, we need only look at the application of paramagnetic MRI contrast agents. Paramagnetic agents only influence protons in their immediate vicinity and removal of these contrast agents by the RES during passive targeting may decrease their effectiveness via two mechanisms: (1) accumulation of contrast agent in specific organs that are distal to region of interest, and (2) endocytosis further decreases their exposure to free water protons. By targeting the contrast agent, the paramagnetic ions can be brought in close proximity to the region of interest with significant accumulation to overcome the partial dilution effect that plagues some MR contrast agents. Its efficacy is further enhanced with some targeting platforms by delivering multiple contrast ions per particle (Lanza, Lorenz et al 1998).

Basic principles of ultrasound contrast agents

Commercially available ultrasound contrast agents are based on gas-filled encapsulated microbubbles (~2.5–5 microns) that transiently enhance the blood pool signal, which is otherwise weakly echogenic. When insonified by an ultrasound wave, microbubbles improve gray scale images and Doppler signal via two distinct mechanisms (Dalla Palma and Bertolotto 1999; McCulloch et al 2000; Correas et al 2001). First, at lower acoustic power, microbubbles are highly efficient scatters due to their large differences in acoustic impedance (Z) compared with surrounding tissue or blood. With increasing acoustic energies, microbubbles begin non-linear oscillations and emit harmonics of the fundamental (incidence) frequencies; thus behaving as a source of sound, rather than as a passive reflector. Biological tissue does not display this degree of harmonic generation, thus the contrast generated signal can be exploited to preferentially image microbubbles and improve signal-to-noise ratios. To emphasize these strong echogenic properties, it has been shown that even one microbubble can be detected with medical ultrasound systems (Klibanov et al 2004). Interestingly, destruction and cavitation of microbubbles by ultrasound waves have been suggested as a means to facilitate drug delivery by "sonoporating" membranes and allowing drugs and gene therapy to enter the cell (Shohet et al 2000; Blomley et al 2001). However, the long term effects on cell viability have yet to be assessed. When this process occurs in capillary beds, permeability increases allowing a subset of particles access to surrounding tissue for further drug deposition et al 1998).

The wide use of microbubbles in everyday clinical applications highlight its effectiveness as a blood pool agent. For example, microbubbles enhance the blood-tissue boundary of the left ventricular cavity allowing for better diagnostic yield in resting as well as stress echocardiograms (Cheng et al 1998). Improved Doppler signals are beneficial in the diagnosis of valvular stenosis and regurgitation (Terasawa et al 1993). Additionally, microbubbles are removed from circulation via the RES and accumulate in the liver and spleen, ie, passive targeting. This mechanism can be employed for the detection of focal liver lesions and malignancies (Harvey et al 2000; Blomley et al 2001). For use as targeted contrast agents, microbubbles have been conjugated with ligands for a variety of vascular biomarkers including integrins expressed during angiogenesis, the glycoprotein IIb/IIIa receptor on activated platelets in clots and L-selectin for the selective enhancement of peripheral lymph nodes in vivo (Schumann et al 2002; Leong-Poi et al 2003; Hauff et al 2004). One disadvantage to the targeting of microbubbles is the "tethering" of these particles to a surface. This interaction with a solid structure limits the ability of insonified microbubbles to oscillate and dampens their echogenicity.

As mentioned previously, we have developed a novel multidimensional targeted nanoparticle platform that is a ligand-targeted, lipid encapsulated, nongaseous perfluorocarbon emulsion. It is robustly stable to handling, pressure, atmospheric exposure, heat and shear forces. Unlike microbubble formulations that are naturally echogenic, these nanoparticles have poor inherent acoustic reflectivity and have been shown to exhibit backscattering levels 30 dB below that of whole blood (Hughes et al 2005). However, when collective deposition occurs on the surfaces of tissues or a cell in a layering effect, these particles create a local acoustic impedance mismatch that produces a strong ultrasound signal without a concomitant increase in the background level (Lanza, Trousil et al 1998). The echogenicity of nanoparticles does not depend upon the generation of harmonics and therefore is not affected by binding of nanoparticles with molecular epitopes. Due to their small size and inherent in vivo stability, perfluorocarbon nanoparticle emulsions have a long circulatory half-life compared to microbubble contrast agents. This is accomplished without modification of their outer lipid surfaces with polyethylene glycol or incorporation of polymerized lipids, which can detract from the targeting efficacy. Data suggest that the PFC nanoparticles persist when bound to tissue for hours and possibly days. Additionally, nongaseous nanoparticles do not easily deform or cavitate with ultrasound imaging.

Basic principles of MR contrast agents

In addition to acoustic imaging, this nanoparticle platform has been coupled to paramagnetic ions for MR imaging. As a dual-modality contrast agent, the strengths of ultrasound imaging, ie, flexibility, portability and ease of use are combined with the high spatial resolution of MR imaging. To understand how nanoparticles can be employed as an MR contrast agent, an understanding of the NMR phenomenon is crucial. The nuclei of elements such as hydrogen (^{1}H) or fluorine (^{19}F), when exposed to a strong magnetic field will change from their random orientation to adopt either a parallel or anti-parallel alignment. Absorption of radiofrequency (RF) energy at a characteristic resonance frequency excites nuclei into a higher energy state. Upon termination of the RF excitation, nuclei return to the previous lower energy state in an exponential fashion with a characteristic rate time constant known as T1 (ie, spin-lattice or longitudinal relaxation). This process of excitation and relaxation results in a changing magnetic field that is detectable with an external RF antenna. This detected signal strength is diminished due to dephasing, which is a process of nuclei to nuclei interactions (ie, spin-spin or transverse relaxation) characterized by the time constant T2. T1 and T2 relaxation times, as well as the density of the nuclei of interest, determine signal intensity of various types of tissue in MR imaging.

MR contrast agents work by shortening T1 and T2. The most commonly used non-targeted MR contrast agents utilize paramagnetic ions (eg, gadolinium chelates) and they predominantly shorten T1 relaxation resulting in a "bright" signal on T1 weighted images. T1 agents chiefly influence protons proximate to themselves and are highly dependent on local water flux (Lanza et al 2004). Superparamagnetic and ferromagnetic compounds have a high magnetic susceptibility and produce local disturbances in the field (Nelson and Runge 1995). These disturbances induce signal dephasing in tissue and result in loss of signal through apparent T2 decay (ie, T2*). Contrary to T1 contrast agents, superparamagnetic agents have a net effect far beyond their immediate vicinity.

For use as a T1 weighted paramagnetic contrast agent, PFC nanoparticles can be functionalized by surface incorporation with homing ligands and typically 100,000 gadolinium chelates (Gd^{3+}) per particle (Flacke et al 2001). In addition, all of the paramagnetic ions are present in the outer surface where they optimally influence the local water for maximum effect on T1 relaxation (Winter, Caruthers et al 2003). The result is PFC nanoparticles that are capable of overcoming the diluting partial volume effects that plague most MR contrast agents (Gupta and Weissleder 1996). To illustrate the potency of this contrast agent platform, we need only examine its relaxivity. The efficiency of an MR contrast agent can be described by its relaxivity ($mM^{-1}sec^{-1}$), which is simply calculated as the change in relaxation rate (1/T1 or T2) divided by the concentration of the contrast agent. The relaxivity of Gd^{3+} in saline (4.5 $mM^{-1}sec^{-1}$) (Stanisz and Henkelman 2000) is lower when compared to Gd^{3+} bound to the surface of a PFC nanoparticles (33.7 $mM^{-1}sec^{-1}$) (Winter, Caruthers et al 2003) at 1.5T. Since each nanoparticle bears high payloads of Gd ions, the overall relaxivity of the construct, also referred to as the particle-based relaxivity, has been measured at over 2,000,000 $mM^{-1}sec^{-1}$ (Winter, Caruthers et al 2003). This allows for detection and quantification of tissue biomarkers at low nanomolar concentrations (Morawski et al 2004).

PFC nanoparticles for fluorine (^{19}F) MR spectroscopy and imaging

The intensity of an MR signal is directly proportional to the gyromagnetic ratio (γ) and density (number of nuclei

in the volume of interest) (Bushong 2003). Though there are many medically relevant nuclei, the ^{1}H proton is the most commonly imaged nuclei in clinical practice because of its high gyromagentic ratio, high natural abundance and high concentrations in biological tissue (see Table 1). Fluorine-19, whose gyromagnetic ratio is close to ^{1}H and has a natural abundance of virtually 100%, is a theoretically attractive nucleus for MR imaging (Longmaid et al 1985). Its sensitivity is 83% when compared to ^{1}H at a constant field strength and with equivalent number of nuclei. In biological tissue, low ^{19}F concentrations (in the range of micromoles) makes MR imaging ineffective without ^{19}F rich contrast agents (McFarland et al 1985). PFC nanoparticles are 98% perfluorocarbon by volume, which equates for perfluorooctylbromide (1.98 g/ml, 498 daltons) to approximately 100M concentration of fluorine within a nanoparticle. The paucity of endogenous fluorine in biological tissue allows the use of exogenous PFC nanoparticles as an effective ^{19}F MR contrast agent without interference from significant background signal. When combined with local drug delivery, detection of the ^{19}F signal serves as a highly specific marker for the presence of nanoparticles that would permit quantitative assessment of drug dosing.

^{19}F has seven outer-shell electrons rather than a single electron as is the case with hydrogen; as a result, the range and sensitivity of chemical shifts to the details of the local environment are much higher for fluorine than hydrogen. Distinct spectra from different perfluorocarbon species can be obtained and utilized for simultaneously distinguishing multiple biochemical markers via MR spectroscopy or imaging (Caruthers et al 2006).

For use as a clinically applicable contrast agent, the biocompatibility of PFC nanoparticles must be reviewed. Liquid PFC were previously developed for use as a blood substitute (Sloviter and Mukherji 1983) and no toxicity, carcinogenicity, mutagenicity or teratogenic effects have been reported for pure fluorocarbons within the 460 to 520 MW range. PFC's are inert biologically and removed through the RES and excreted primarily through the lungs and in small amounts through the skin (Joseph et al 1985). Tissue half-life ranges from 4 days for perfluorooctylbromide up to 65 days for perfluorotripropylamine. The prolonged systemic half-life of PFC nanoparticles in conjunction with the local concentrating effect produced by ligand-directed binding, permit ^{19}F spectroscopy and imaging studies at clinically relevant magnetic field strengths (Yu et al 2000).

Table 1 MRI properties of clinically important nuclei

Nuclei	Gyromagnetic ratio (MHz/T)	Spin quantum number	Natural abundance (%)	Relative sensitivity
^{1}H	42.6	1/2	99	1.0
^{13}C	10.7	1/2	1.1	0.016
^{17}O	5.8	5/2	0.1	0.029
^{19}F	40.0	½	100	0.83
^{23}Na	11.3	3/2	100	0.093
^{31}P	17.2	1/2	100	0.07

Fibrin-imaging for detection of unstable plaque and thrombus

Of the over 720,000 cardiac related deaths per year in the United States, roughly 63% are classified as sudden cardiac death (SCD) (Zheng et al 2001). Unfortunately for many patients, this is the first and only symptom of their atherosclerotic heart disease (ASHD) (Kuller et al 1966). Atherosclerosis begins as a fatty streak and without proper treatment, it can progress to a vulnerable plaque characterized by a large lipid core, thin fibrous cap and macrophage infiltrates (Naghavi 2003). These vulnerable plaques are prone to rupture which can lead to thrombosis, vascular occlusion and subsequent myocardial infarction (Davies and Thomas 1985) or stroke. Routine angiography is the most common method of diagnosing ASHD with identification of high grade lesions (>70% stenosis) being referred for immediate therapeutic intervention. Ironically, most ruptured plaques originate from coronary lesions classified as "non-stenotic" (Naghavi et al 2003). Even nuclear and US based stress test are only designed to detect flow limiting lesions. Because the most common source of thromboembolisms come from atherosclerotic plaques with 50%–60% stenosis (Ambrose et al 1988), diagnosis by traditional techniques remains elusive. In addition, there appears to be a "window of opportunity" that exists between the detection of a vulnerable or ruptured plaque and acute myocardial infarction (a few days to months) (Ojio et al 2000) in which intervention could prove to be beneficial.

Acoustic enhancement of thrombi using fibrin targeted nanoparticles was first demonstrated in vitro as well as in vivo in a canine model at frequencies typically used in clinical transcutaneous scanning (Lanza et al 1996). Detection of thrombi was later expanded to MRI in a study by Flacke et al (2001). Fibrin clots were targeted in vitro with paramagnetic nanoparticles and imaged using typical "low" resolution T1 proton imaging protocols (gradient and spin echo) at 1.5T. Low resolution images show enhancement of MR signal by the PFC nanoparticles and appear to completely fill the clot volume (see Figure 3). However, at higher in-plane resolution, the same clot

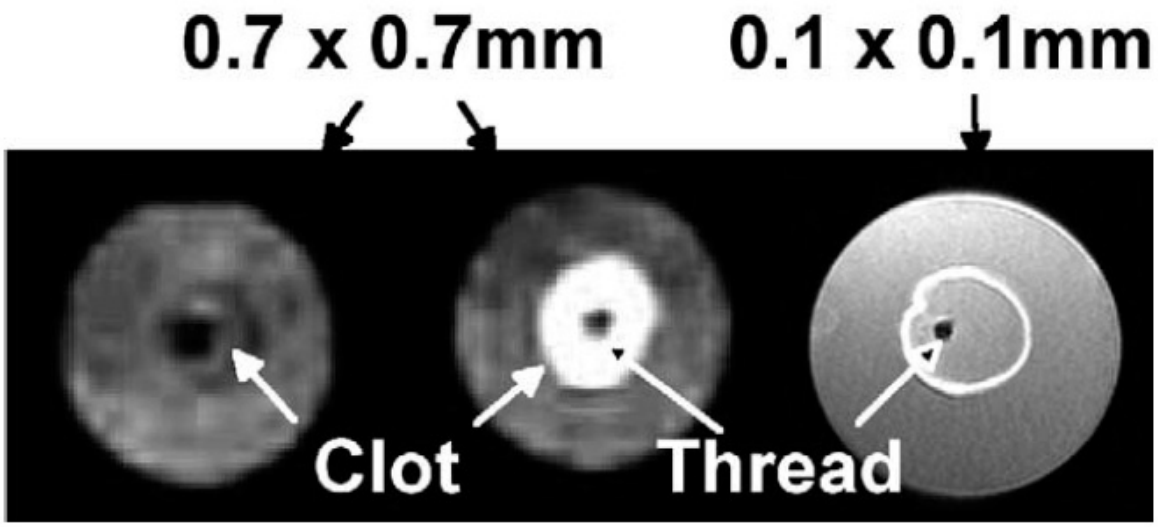

Figure 3 (Left) Low-resolution images (3D gradient and spin echo) of control and (Middle) fibrin-targeted clot with paramagnetic nanoparticles presenting a homogenous, T1-weighted enhancement. (Right) High resolution scans of fibrin clots (3D T1-weighted gradient recalled echo sequence), revealing that image B results from a thin layer of paramagnetic nanoparticles along the surface. Copyright © 2001. Reprinted with permission from Flacke S, Fischer S, et al. 2001. Novel MRI contrast agent for molecular imaging of fibrin: implications for detecting vulnerable plaques. *Circulation*, 104:1280–5.

reveals that the nanoparticles were bound only at the surface and were excluded from penetration into the dense fibrin matrix (see Figure 1). In the same study, in vivo MR images were obtained of fibrin clots in the external jugular vein of dogs. Enhancement with fibrin targeted PFC nanoparticles produced high signal intensity in treated clots (1780 ± 327), whereas the control clot had a signal intensity (815 ± 41) similar to that of the adjacent muscle (768 ± 47). This method was extended to the detection of ruptured plaque in human carotid artery endarterectomy specimens resected from a symptomatic patient (see Figure 4). Fibrin deposition was localized to the shoulders of the ruptured plaque in the targeted vessel but this was not appreciated in the control. Further investigation in the molecular imaging of fibrin in ruptured plaque may someday detect this silent pathology sooner in order to preempt stroke or myocardial infarction.

The high fluorine content of fibrin-targeted PFC nanoparticles as well as the lack of background signal were exploited for ^{19}F MR imaging and spectroscopy. In a recent study, Morawski et al (2004) describe several methods for quantifying the number of nanoparticles bound to a fibrin clot using the ^{19}F signal. First, fibrin-targeted paramagnetic perfluoro-crown-ether nanoparticles and trichlorofluoromethane ^{19}F spectra were obtained (Figure 5a). The relative crown ether signal intensity (normalized to the external trichlorofluoromethane reference) from known emulsion volumes provided a calibration curve for nanoparticle quantification (Figure 5b). The PFC (crown ether) nanoparticles were then mixed in titrated ratios with fibrin-targeted nanoparticles containing safflower oil and bound to plasma clots in vitro. As the competing amount of safflower agent was increased, there was a linear decrease in ^{19}F signal. Bound NP was calculated from the ^{19}F signal and the calibration curve described above and compared with the mass of Gd^{3+} tracer as determined by neutron activitation analysis. As expected, there was excellent agreement between measured Gd^{3+} mass and number of bound nanoparticles (calculated from the ^{19}F signal) (see Figure 5c).

In addition, clots were treated with fibrin targeted nanoparticles with two distinct perfluorocarbon cores, crown ether and PFOB (Morawski et al 2004). They both exhibited

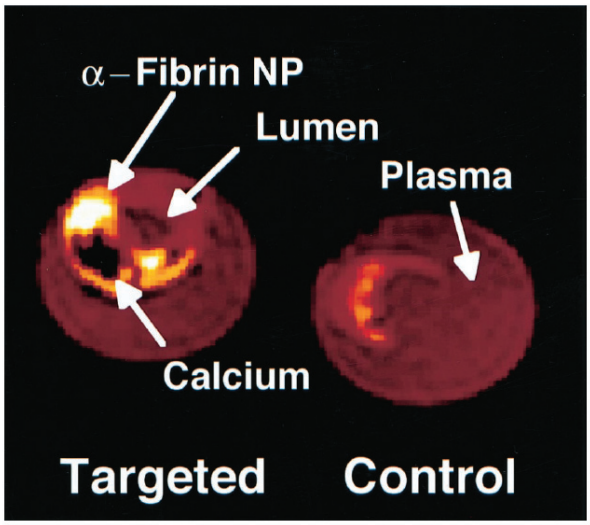

Figure 4 Color enhanced magnetic resonance imaging of fibrin-targeted and control carotid endarterectomy speciments revealing contrast enhancement (white) of a small fibrin deposit on a symptomatic ruptured plaque. Calcium deposit (black). 3D, fat-suppressed, T1-weighted fast gradient echo. Copyright © 2001. Reprinted with permission from Flacke S, Fischer S, et al. 2001. Novel MRI contrast agent for molecular imaging of fibrin: implications for detecting vulnerable plaques. *Circulation*, 104:1280–5.

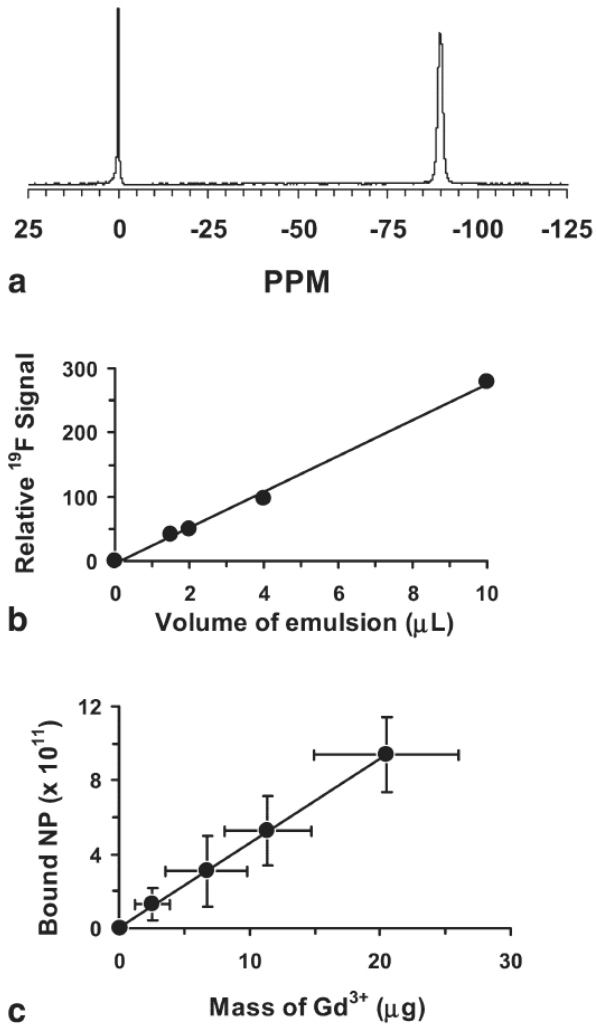

Figure 5 (**a**) Representative spectrum taken at 4.7 T of crown ether emulsion (~90 ppm) and trichlorofluormethane (0 ppm) used as a reference. (**b**) The calibration curve for crown ether emulsion has a slope of 28.06 with an r^2 of 0.9968. (**c**) The calculated number of bound nanoparticles (mean ± standard error, n = 3) as calculated from ^{19}F spectroscopy versus the mass of total gadolinium (Gd^{3+}) in the sample as determined by neutron activation analysis show excellent agreement as independent measures of fibrin-targeted nanoparticles binding to clots. The linear regression line has an r^2 of 0.9997. Copyright © 2004. Reprinted with permission from Morawski AM, Winter PM, et al. 2004. Targeted nanoparticles for quantitative imaging of sparse molecular epitopes with MRI. *Magnetic Resonance in Medicine*, 51:480–6.

two distinct ^{19}F spectra at 4.7T and the binding of each respective nanoparticles was highly related to the ratio of PFOB and crown ether emulsion applied. These findings demonstrate the possibility of simultaneous imaging and quantifying two separate nanoparticles and hence two distinct biomarkers (Caruthers et al 2006).

The clinical exercise of these techniques was applied to the analysis of human carotid endarterectomy samples (see Figure 6). An optical image of the carotid revealed extensive plaques, wall thickening and luminal irregularities. Multi-slice ^{1}H images showed high levels of signal enhancement along the luminal surface due to binding of targeted paramagnetic nanoparticles to fibrin deposits (not shown in Figure 6). ^{19}F projection images of the artery, taken in approximately 5 min, showed an asymmetric distribution of fibrin-targeted nanoparticles around the vessel wall corroborating the signal enhancement observed with ^{1}H MRI. Concomitant visualization of ^{1}H and ^{19}F images would permit the visualization of anatomical and pathological information in a single image. In theory, atherosclerotic plaque burden could be visualized with paramagnetic PFC contrast enhanced ^{1}H images while ^{19}F could locally identify plaques with high levels of fibrin and thus prone to rupture. This simultaneous information could improve treatment strategies.

Detection of angiogenesis and vascular injury

As described previously, ligand-directed PFC nanoparticles are well suited to detect very sparse biomarkers, such as integrins involved in the process of angiogenesis. Angiogenesis is a critical component in wound healing, inflammation and development; but also contributes to the pathology of many disease processes such as diabetic retinopathy, rheumatoid arthritis, cancer and atherosclerosis. The process of angiogenesis depends upon the adhesion interactions of vascular cells and the integrin $\alpha_v\beta_3$ has been identified as playing a vital role in angiogenic vascular tissue. The function of $\alpha_v\beta_3$ includes smooth muscle cell (SMC) migration and proliferation, vascular cell apoptosis, and vascular remodeling (Sajid and Stouffer 2002) and it is expressed on the luminal surface of activated endothelial cells but not on mature quiescent cells. These findings support that the role of $\alpha_v\beta_3$ in pathological conditions characterized by neovascularization may be an important diagnostic and therapeutic target. In fact, the use of a monoclonal antibody against $\alpha_v\beta_3$ has demonstrated inhibition of angiogenesis without affecting mature vessels (Brooks et al 1994).

PFC nanoparticles have been developed to detect the sparse expression of the $\alpha_v\beta_3$ integrin on the neovasculature (Anderson et al 2000) and to deliver anti-angiogenic therapy. This has been utilized in New Zealand white rabbits bearing Vx-2 tumors (<1.0 cm) at 1.5T (Winter, Caruthers et al 2003). MRI signal 2 h post injection of $\alpha_v\beta_3$-targeted nanoparticles revealed signal enhancement of 126% predominantly in an asymmetrical distribution along the tumor border. These results paralleled the immunohistochemical staining results. Moreover, in vivo competitive blocking with $\alpha_v\beta_3$ targeted non-paramagnetic nanoparticles resulted in decreased signal enhancement to a level attributable to

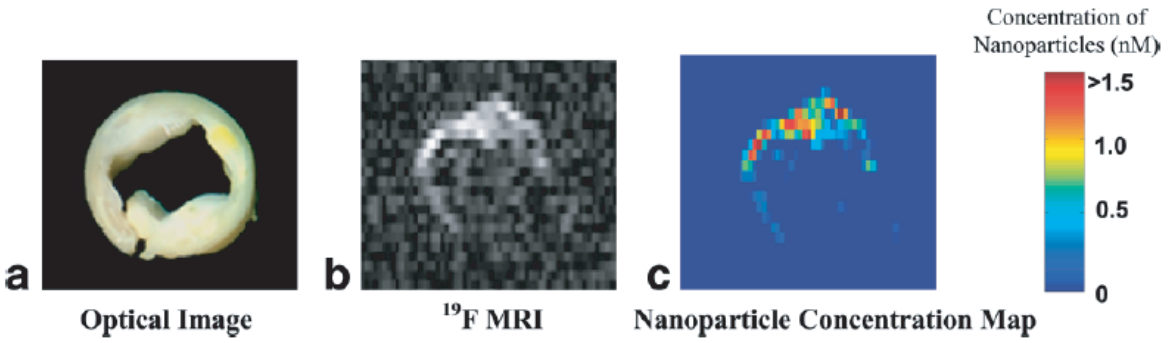

Figure 6 (**a**) Optical image of a 5-mm cross-section of a human carotid endarterectomy sample. This section showed moderate luminal narrowing as well as several atherosclerotic lesions. (**b**) A ^{19}F projection image acquired at 4.7 T through the entire carotid artery sample shows high signal along the lumen due to nanoparticles bound to fibrin. (**c**) Concentration map of bound nanoparticles in the carotid sample. Copyright © 2004. Reprinted with permission from Morawski AM, Winter PM, et al. 2004. Targeted nanoparticles for quantitative imaging of sparse molecular epitopes with MRI. *Magnetic Resonance in Medicine*, 51:480–6.

local extravasation. In an analogous study, athymic nude mice bearing human melanoma tumors (C32, ATCC; ~33mm^3) were injected with $\alpha_v\beta_3$ targeted PFC nanoparticles and imaged at 2 h (Schmieder, Winter et al. 2005). MR enhancement was apparent within 0.5 h and increased by 173% at 2 h (see Figure 7). Again, MR imaging results were corroborated with histological results. In both studies, in vivo competitive blocking with $\alpha_v\beta_3$ targeted non-paramagnetic nanoparticles inhibited the evolution of the targeted signal. These findings speak to the high specificity achievable with $\alpha_v\beta_3$ targeted nanoparticles.

Angiogenesis also plays a crucial and early role in the pathogenesis of atherosclerosis and the inhibition of angiogenesis has been shown to decrease plaque progression (Moulton et al 1999, 2003). Unfortunately, detection of atherosclerosis generally does not occur until late stages of the disease when a clinical event is caused by a plaque rupture. Conventional noninvasive imaging techniques are not sensitive or specific enough to detect the sparse biomarkers associated with early atherosclerosis. However, $\alpha_v\beta_3$-targeted paramagnetic nanoparticles have been demonstrated to spatially localize and quantify neovascularization associated with early atherosclerosis in hyperlipidemic New Zealand White rabbits (see Figure 8) (Winter, Morawski et al 2003).

In addition to angiogenesis, $\alpha_v\beta_3$ has an important role in the development of restenosis following balloon injury from angioplasty. It is expressed following vascular injury and facilitates smooth muscle migration and proliferation, cell adhesion to the extracellular matrix as well as induction of extracellular metalloproteinase expression. Multiple animal studies have shown that IV administration of $\alpha_v\beta_3$ antagonism following balloon angioplasty results in decreased neointimal growth and lumen stenosis (Srivatsa et al 1997; Bishop et al 2001). We have developed a high avidity $\alpha_v\beta_3$ integrin specific nanoparticle that can target $\alpha_v\beta_3$ integrin exposed on smooth muscle cells by arterial overstretch injury and provide new prognostic data relating the extent and severity of balloon injury as well as facilitate the delivery of therapeutic agents from within the damaged arterial wall (Cyrus et al 2003).

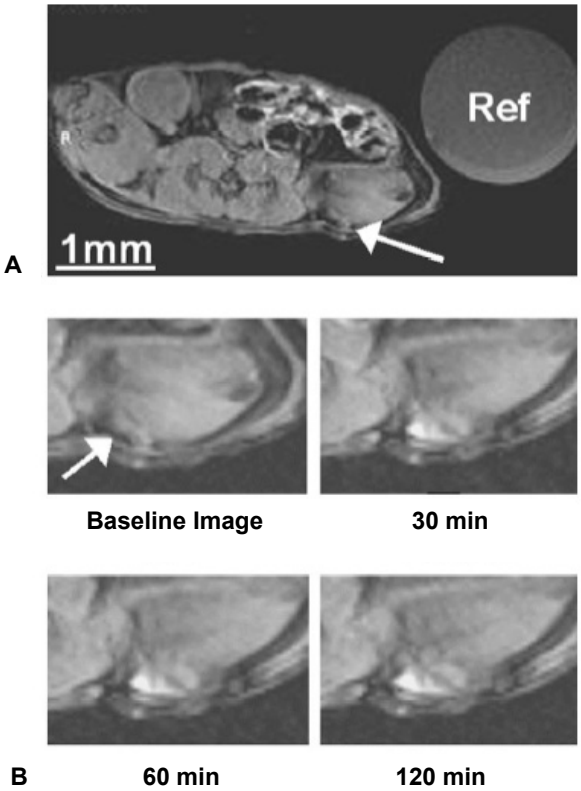

Figure 7 (**A**) T1-weighted MR image (axial view) of an athymic nude mouse before injection of paramagnetic $\alpha v\beta_3$-targeted nanoparticles. Arrow indicates a C32 tumor that is difficult to detect ("Ref" = Gd^{3+} DTPA in 10 cc syringe). (**B**) Enlarged section of an MR image showing T1-weighted signal enhancement of angiogenic vasculature of early tumors over 2 h as detected by $\alpha v\beta_3$-targeted nanoparticles. Copyright © 2005. Reprinted with permission from Schmieder AH, Winter PM, et al. 2005. Molecular MR imaging of melanoma angiogenesis with alphanubeta3-targeted paramagnetic nanoparticles. *Magnetic Resonance in Medicine*, 53:621–7.

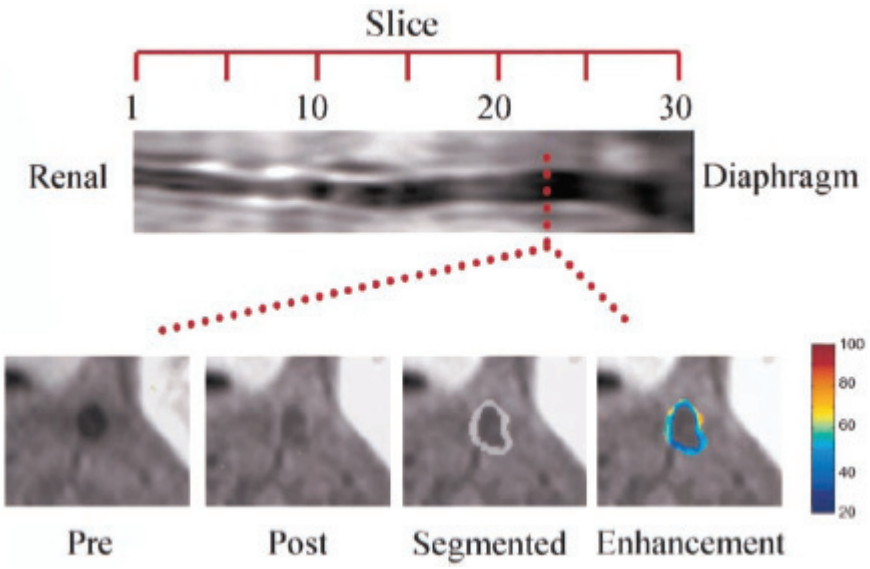

Figure 8 In vivo spin-echo image reformatted to display long axis of aorta from renal arteries to diaphragm of a cholesterol-fed rabbit (top) and at single transverse level (bottom) before (Pre) and after (Post) treatment, after semi-automated segmentation (Segmented, grayish ring), and with color-coded signal enhancement (Enhancement) above baseline (in percent). Copyright © 2003. Reprinted with permission from Winter PM, Morawski AM, et al. 2003. Molecular imaging of angiogenesis in early-stage atherosclerosis with alpha(v)beta3-integrin-targeted nanoparticles. *Circulation*, 108:2270–4.

Similar to $\alpha_v\beta_3$, collagen III is omni-present within the vascular wall and accessible immediately after balloon injury for targeted delivery of therapeutic paramagnetic nanoparticles. We have covalently coupled a monoclonal Fab fragment specific for collagen III to target nanoparticles into carotid extracellular matrix following balloon overstretch injury in pigs, analogous to the studies previously described for $\alpha_v\beta_3$-targeted paramagnetic nanoparticles (Cyrus et al 2003).

Contact facilitated drug delivery

Besides detecting sparse epitopes for non-invasive imaging, PFC nanoparticles are capable of specifically and locally delivering drugs and other therapeutic agents through a novel process known as contact facilitated drug delivery (Lanza et al 2004). Direct transfer of lipids and drugs from the outer surfactant layer to the cell membrane of the targeted cell is usually a slow and inefficient process. Through ligand directed targeting, this

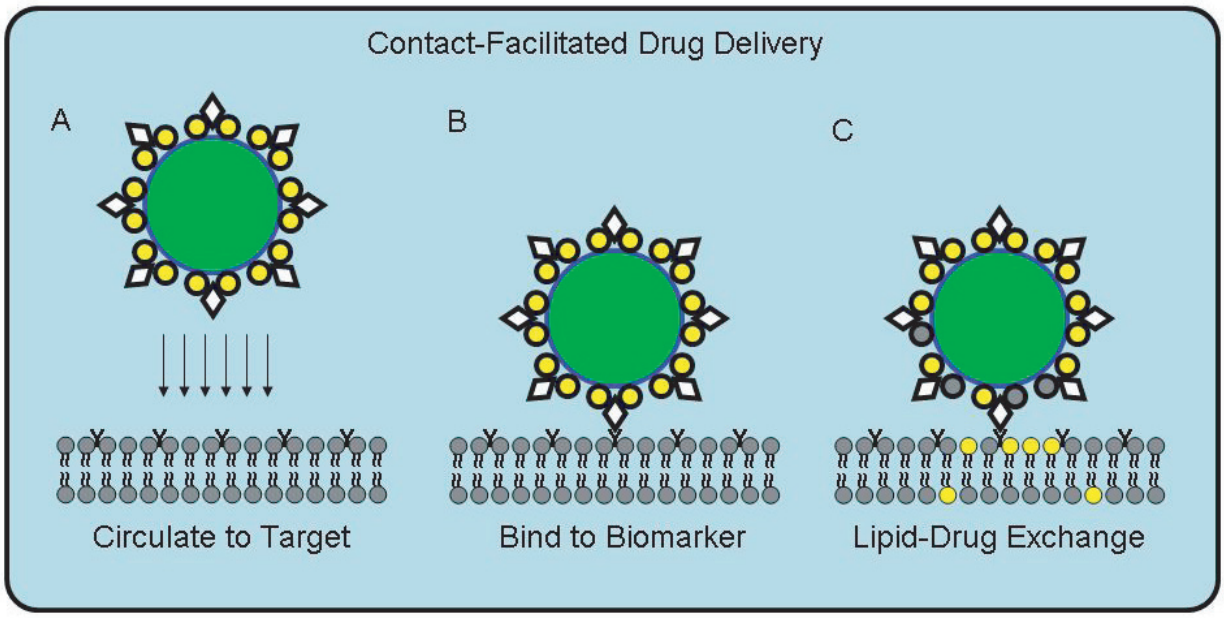

Figure 9 Schematic representation illustrating contact-facilitated drug delivery. Phospholipids and drug within the nanoparticles surfactant exchange with lipids of the target membrane through a convection process, rather than diffusion, as is common among other targeted systems. Copyright © 2004. Reprinted with permission from Lanza GM, Winter PM, et al. 2004. Magnetic resonance molecular imaging with nanoparticles. *Journal of Nuclear Cardiology*, 11:733–43.

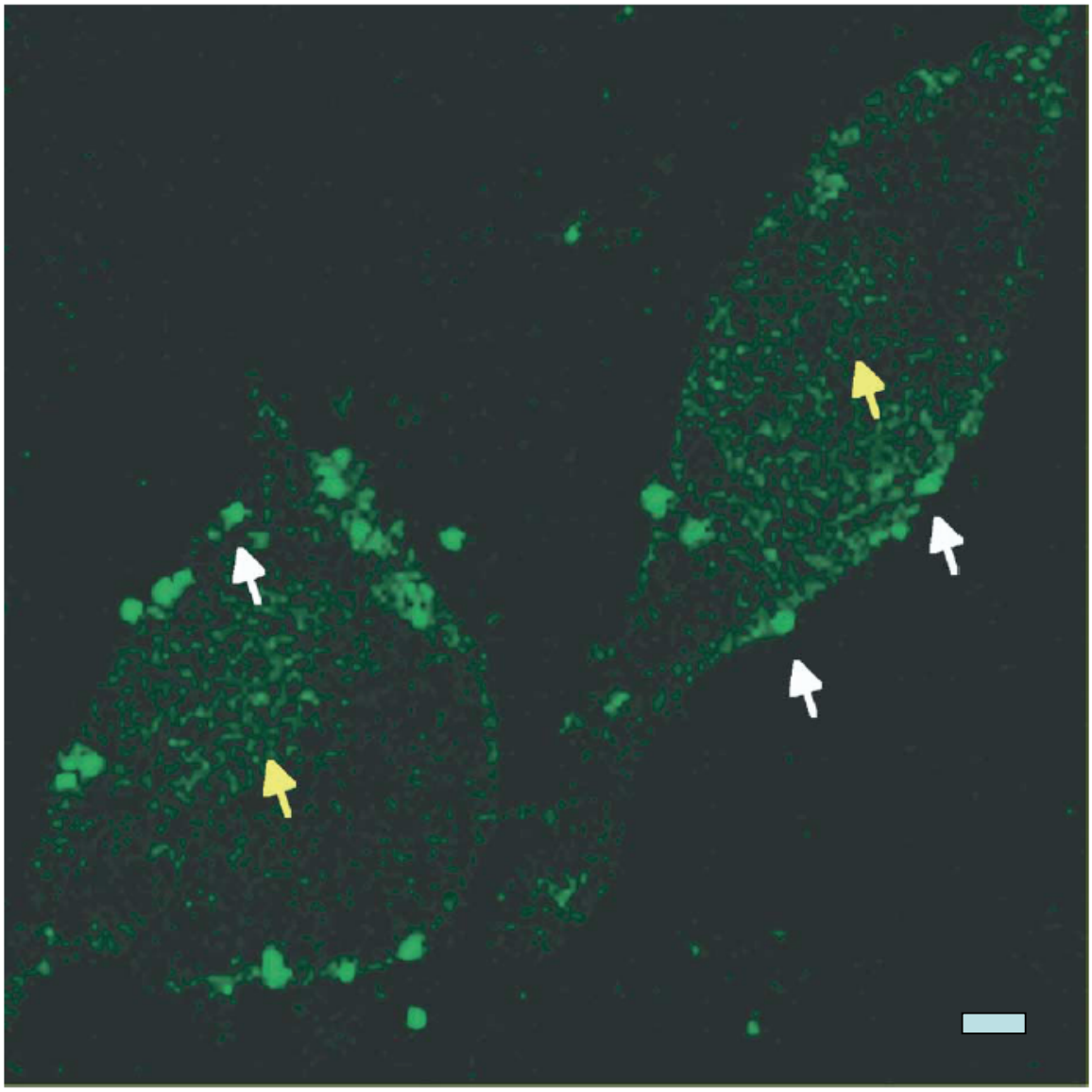

Figure 10 In vitro targeting of FITC-labeled nanoparticles (white arrows) targeted to avb3-integrin expressed by C-32 melanoma cells, which illustrate the delivery of FITC-labeled surfactant lipids into target cell membranes (yellow arrows). Scale bar = 2 microns. Copyright © 2004. Reprinted with permission from Lanza GM, Winter PM, et al. 2004. Magnetic resonance molecular imaging with nanoparticles. *Journal of Nuclear Cardiology*, 11:733–43.

process is accelerated by minimizing the separation of the lipids surfaces and increasing the frequency and duration of the lipid surface interactions (see Figures 9 and 10). Spatial localization (via high resolution ^{1}H MR imaging) and quantification of the nanoparticles (via ^{19}F spectroscopy) permits the local therapeutic concentrations to be estimated. Thus, PFC nanoparticles can be used for detection, therapy and treatment monitoring.

As an example, in vitro vascular smooth muscle cells were treated with tissue-factor targeted PFC nanoparticles containing 0, 0.2, or 2.0 mole % doxorubicin or paclitaxel or an equivalent amount of drug in buffer solution alone (Lanza, Yu et al 2002). With only targeting for 30 minutes, proliferation measured at 72 hours was inhibited. High resolution MR imaging with 4.7T revealed the image intensity of the targeted VSCM's was 2-fold higher as compared with nontargeted cells. In addition, the fluorine signal amplitude at 0.47T was linearly correlated to the perfluorocarbon concentrations, which by direct inference could be related to nanoparticles number.

Conclusion

Ligand-directed liquid PFC nanoparticles are an extremely versatile imaging platform that permit noninvasive assessment of clinically important sparce biomarkers, such as integrins in angiogenesis as well as high density epitopes, such as fibrin. The unique properties of targeted nanoparticles present the opportunity to diagnose, deliver therapy

and predict therapeutic response with a single platform. Furthermore, they allow image based serial monitoring. Their impact in the fields of cardiology and oncology are predicted to be profound.

References

Ambrose JA, Tannenbaum MA, et al. 1988. Angiographic progression of coronary artery disease and the development of myocardial infarction. *Journal of the American College of Cardiology*, 12:56–62.

Anderson SA, Rader RK, et al. 2000. Magnetic resonance contrast enhancement of neovasculature with alpha(v)beta(3)-targeted nanoparticles. *Magnetic Resonance in Medicine*, 44:433–9.

Bishop GG, McPherson JA, et al. 2001. Selective alpha(v)beta(3)-receptor blockade reduces macrophage infiltration and restenosis after balloon angioplasty in the atherosclerotic rabbit. *Circulation*, 103:1906–11.

Blomley MJ, Cooke JC, et al. 2001. Microbubble contrast agents: a new era in ultrasound. *BMJ*, 322:1222–5.

Brooks PC, Clark RA, et al. 1994. Requirement of vascular integrin alpha v beta 3 for angiogenesis. *Science*, 264:569–71.

Bushong SC. 2003. Magnetic resonance imaging: physical and biological principles. Saint Louis: *Mosby*.

Caruthers SD, Neubauer AM, et al. 2006. In Vitro Demonstration Using 19F Magnetic Resonance to Augment Molecular Imaging with Paramagnetic Perfluorocarbon Nanoparticles at 1.5 Tesla. *Investigative Radiology*, 41:305–12.

Cheng SC, Dy TC, et al. 1998. Contrast echocardiography: review and future directions. *American Journal of Cardiology*, 81:41G–48G.

Correas JM, Bridal L, et al. 2001. Ultrasound contrast agents: properties, principles of action, tolerance, and artifacts. *European Radiology*, 11:1316–28.

Cyrus T, Caruthers S, et al. In Press. Nanoparticles for magnetic resonance imaging of cancer. In Challa S, Kumar SR. Nanomaterials for cancer therapy and diagnosis. WILEY ~ VCH 6.

Cyrus T, Winter P, et al. 2003. Molecular imaging of avB3-integrin and collagen-III targeted nanoparticles in pig carotids following balloon-inflation injury. *Molecular Imaging*, 2:281.

Dalla Palma L, Bertolotto M. 1999. Introduction to ultrasound contrast agents: physics overview. *European Radiology*, 9(Suppl 3):S338–42.

Davies MJ, Thomas AC. 1985. Plaque fissuring – the cause of acute myocardial infarction, sudden ischaemic death, and crescendo angina. *British Heart Journal*, 53(4):363–73.

Flacke S, Fischer S, et al. 2001. Novel MRI contrast agent for molecular imaging of fibrin: implications for detecting vulnerable plaques. *Circulation*, 104:1280–5.

Gupta H, Weissleder R. 1996. Targeted contrast agents in MR imaging. *Magnetic Resonance Imaging Clinics of North America*, 4:171–84.

Harvey CJ, Blomley MJ, et al. 2000. Hepatic malignancies: improved detection with pulse-inversion US in late phase of enhancement with SH U 508A-early experience. *Radiology*, 216:903–8.

Hauff P, Reinhardt M, et al. 2004. Molecular targeting of lymph nodes with L-selectin ligand-specific US contrast agent: a feasibility study in mice and dogs.[see comment]. *Radiology*, 231:667–73.

Hughes MS, Marsh JN, et al. 2005. Acoustic characterization in whole blood and plasma of site-targeted nanoparticle ultrasound contrast agent for molecular imaging. *Journal of the Acoustical Society of America*, 117:964–72.

Joseph PM, Yuasa Y, et al. 1985. Magnetic resonance imaging of fluorine in rats infused with artificial blood. *Investigative Radiology*, 20:504–9.

Klibanov AL, Rasche PT, et al. 2004. Detection of individual microbubbles of ultrasound contrast agents: imaging of free-floating and targeted bubbles. *Investigative Radiology*, 39:187–95.

Kuller L, Lilienfeld A, et al. 1966. Epidemiological study of sudden and unexpected deaths due to arteriosclerotic heart disease. *Circulation*, 34:1056–68.

Lanza GM, Lorenz CH, et al. 1998. Enhanced detection of thrombi with a novel fibrin-targeted magnetic resonance imaging agent. *Academic Radiology*, 5(Suppl 1):S173–6; discussion S183–4.

Lanza GM, Trousil RL, et al. 1998. In vitro characterization of a novel, tissue-targeted ultrasonic contrast system with acoustic microscopy. *Journal of the Acoustical Society of America*, 104:3665–72.

Lanza GM, Wallace KD, et al. 1996. A novel site-targeted ultrasonic contrast agent with broad biomedical application. *Circulation*, 94:3334–40. [Erratum appears in *Circulation* 1997 May 20;95:2458.]

Lanza GM, Winter PM, et al. 2004. Magnetic resonance molecular imaging with nanoparticles. *Journal of Nuclear Cardiology*, 11:733–43.

Lanza GM, Yu X, et al. 2002. Targeted antiproliferative drug delivery to vascular smooth muscle cells with a magnetic resonance imaging nanoparticle contrast agent: implications for rational therapy of restenosis. *Circulation*, 106:2842–7.

Leong-Poi H, Christiansen J, et al. 2003. Noninvasive assessment of angiogenesis by ultrasound and microbubbles targeted to alpha(v)-integrins. *Circulation*, 107:455–60.

Longmaid HE 3rd, Adams DF, et al. 1985. In vivo 19F NMR imaging of liver, tumor, and abscess in rats. Preliminary results. *Investigative Radiology*, 20:141–5.

McCulloch M, Gresser C, et al. 2000. Ultrasound contrast physics: A series on contrast echocardiography, article 3. *Journal of the American Society of Echocardiography*, 13:959–67.

McFarland E, Koutcher JA, et al. 1985. In vivo 19F NMR imaging. *Journal of Computer Assisted Tomography*, 9:8–15.

Moghimi SM, Patel HM. 1989. Serum opsonins and phagocytosis of saturated and unsaturated phospholipid liposomes. *Biochimica et Biophysica Acta*, 984:384–7.

Morawski AM, Winter PM, et al. 2004. Targeted nanoparticles for quantitative imaging of sparse molecular epitopes with MRI. *Magnetic Resonance in Medicine*, 51:480–6.

Morawski AM, Winter PM, et al. 2004b. Quantitative magnetic resonance immunohistochemistry with ligand-targeted (19)F nanoparticles. *Magnetic Resonance in Medicine*, 52:1255–62.

Moulton KS, Heller E, et al. 1999. Angiogenesis inhibitors endostatin or TNP-470 reduce intimal neovascularization and plaque growth in apolipoprotein E-deficient mice [see comment]. *Circulation*, 99:1726–32.

Moulton KS, Vakili K, et al. 2003. Inhibition of plaque neovascularization reduces macrophage accumulation and progression of advanced atherosclerosis. *Proceedings of the National Academy of Sciences of the United States of America*, 100:4736–41.

Naghavi M, Libby P, et al. 2003. From vulnerable plaque to vulnerable patient: a call for new definitions and risk assessment strategies: Part I. *Circulation*, 108:1664–72.

Nelson KL, Runge VM. 1995. Basic principles of MR contrast. *Topics in Magnetic Resonance Imaging*, 7:124–36.

Ojio S, Takatsu H, et al. 2000. Considerable time from the onset of plaque rupture and/or thrombi until the onset of acute myocardial infarction in humans: coronary angiographic findings within 1 week before the onset of infarction [see comment]. *Circulation*, 102:2063–9.

Price RJ, Skyba DM, et al. 1998. Delivery of colloidal particles and red blood cells to tissue through microvessel ruptures created by targeted microbubble destruction with ultrasound. *Circulation*, 98:1264–7.

Sajid M, Stouffer GA. 2002. The role of alpha(v)beta3 integrins in vascular healing. *Thrombosis & Haemostasis*, 87:187–93.

Schmieder AH, Winter PM, et al. 2005. Molecular MR imaging of melanoma angiogenesis with alphanubeta3-targeted paramagnetic nanoparticles. *Magnetic Resonance in Medicine*, 53:621–7.

Schumann PA, Christiansen JP, et al. 2002. Targeted-microbubble binding selectively to GPIIb IIIa receptors of platelet thrombi. *Investigative Radiology*, 37:587–93.

Shohet RV, Chen S, et al. 2000. Echocardiographic destruction of albumin microbubbles directs gene delivery to the myocardium. *Circulation*, 101:2554–6.

Sloviter HA, Mukherji B. 1983. Prolonged retention in the circulation of emulsified lipid-coated perfluorochemicals. *Progress in Clinical and Biological Research*, 122:181–7.

Srivatsa SS, Fitzpatrick LA, et al. 1997. Selective alpha v beta 3 integrin blockade potently limits neointimal hyperplasia and lumen stenosis following deep coronary arterial stent injury: evidence for the functional importance of integrin alpha v beta 3 and osteopontin expression during neointima formation. *Cardiovascular Research*, 36:408–28.

Stanisz GJ, Henkelman RM. 2000. Gd-DTPA relaxivity depends on macromolecular content. *Magnetic Resonance in Medicine*, 44:665–7.

Terasawa A, Miyatake K, et al. 1993. Enhancement of Doppler flow signals in the left heart chambers by intravenous injection of sonicated albumin. *Journal of the American College of Cardiology*, 21:737–42.

Winter PM, Caruthers SD, et al. 2003. Molecular imaging of angiogenesis in nascent Vx-2 rabbit tumors using a novel alpha(nu)beta3-targeted nanoparticle and 1.5 tesla magnetic resonance imaging. *Cancer Research*, 63:5838–43.

Winter PM, Caruthers SD, et al. 2003. Improved molecular imaging contrast agent for detection of human thrombus. *Magnetic Resonance in Medicine*, 50:411–6.

Winter PM, Morawski AM, et al. 2003. Molecular imaging of angiogenesis in early-stage atherosclerosis with alpha(v)beta3-integrin-targeted nanoparticles. *Circulation*, 108:2270–4.

Yu X, Song SK, et al. 2000. High-resolution MRI characterization of human thrombus using a novel fibrin-targeted paramagnetic nanoparticle contrast agent. *Magnetic Resonance in Medicine*, 44:867–72.

Zheng ZJ, Croft JB, et al. 2001. Sudden cardiac death in the United States, 1989 to 1998 [see comment]. *Circulation*, 104:2158–63.